Methane emissions from Alaska in 2012 from CARVE airborne observations

Methane emissions from Alaska in 2012 from CARVE airborne observations

Rachel Y.-W. Chang [*] [†], Charles E. Miller [‡], Steven J. Dinardo [‡], Anna Karion [§] [¶] Colm Sweeney [§] [¶], Bruce C. Daube [*], John M. Henderson [‖], Marikate E. Mountain [‖], Janusz Eluszkiewicz [‖], John B. Miller [§] [¶], Lori M. Bruhwiler [§], and Steven C. Wofsy [*]

[*]School of Engineering and Applied Sciences, Harvard University, 24 Oxford Street, Cambridge, Massachusetts, 02138 USA,[‡]Jet Propulsion Laboratory, California Institute of Technology, 4800 Oak Grove Drive, Pasadena, California, 91109, USA,[§]NOAA Earth Systems Research Laboratory, Global Monitoring Division, 325 Broadway, Boulder, Colorado, 80305, USA,[¶]Cooperative Institute for Research in Environmental Sciences, University of Colorado, Boulder, Colorado, 80309, USA,[‖]Atmospheric and Environmental Research, Inc., 131 Hartwell Avenue, Lexington, Massachusetts, 02421, USA, and [†]now at Department of Physics and Atmospheric Science, Dalhousie University, 6310 Coburg Road, Halifax, Nova Scotia, B3H 4R2, Canada

Submitted to Proceedings of the National Academy of Sciences of the United States of America

We determined methane (CH_4) emissions from Alaska, USA using airborne measurements from the Carbon Arctic Reservoirs Vulnerability Experiment (CARVE). Atmospheric sampling was conducted between May and September 2012, and analyzed using a customized version of the Polar Weather Research and Forecast model linked to a Lagrangian particle dispersion model (Stochastic Time-Inverted Lagrangian Transport Model). We estimated growing season CH_4 fluxes of 8 ± 2 mg CH_4 m^{-2} d^{-1} averaged over all of Alaska, corresponding to fluxes from wetlands of 56^{+22}_{-13} mg CH_4 m^{-2} d^{-1} if we assumed that wetlands are the only source from the land surface (all uncertainties are 95% confidence intervals from a bootstrapping analysis). Fluxes roughly doubled from May to July, then decreased gradually in August and September. Integrated emissions totaled 2.1 ± 0.5 Tg CH_4 for Alaska from May to September 2012, close to the average (2.3, range 0.7-6 Tg CH_4) predicted by various land surface models and inversion analyses for the growing season. Methane emissions from boreal Alaska were larger than from the North Slope; the monthly regional flux estimates show no evidence of enhanced emissions during early spring or late fall, although these bursts may be more localized in time and space than can be detected by our analysis. These results provide an important baseline to which future studies can be compared.

Methane | Alaska | Tundra | Arctic | Boreal

Significance Statement

Alaska emitted 2.1±0.5 Tg CH_4 during the 2012 growing season, an unexceptional amount despite widespread permafrost thaw and other evidence of climate change in the region. Our results are based on more than 30 airborne measurement flights conducted by the Carbon in Arctic Reservoirs Vulnerability Experiment from May to September 2012 over Alaska. Methane emissions peaked in summer and remained high in the fall. Emissions from boreal regions were notably larger than from North Slope tundra. This is the first regional study of methane emissions from Arctic and boreal regions over a growing season. Our estimates reinforce and refine global models, and they provide an important baseline against which to measure future changes associated with climate change.

Introduction

Recent studies have raised concerns about an increase in methane (CH_4) emissions from Arctic regions as temperatures warm [1, 2, 3]. Carbon stocks in polar regions are estimated to be as large as 1700 Pg of organic carbon [4], preserved by cold, wet conditions that inhibit decomposition. Over the last 20 years, temperatures have increased more rapidly at these latitudes than the rest of the world [5]; continuation of this trend will lead to permafrost warming and thawing [6], potentially releasing vast quantities of carbon dioxide (CO_2) and CH_4 to the atmosphere [7, 8, 9, 10]. A recent synthesis of carbon emissions predicted by permafrost models reported releases in the range of 120±85 Pg C by 2100[11]. Large uncertainties are likewise associated with estimates of CH_4 emissions (12-90 Tg CH_4 yr^{-1})[12]. The potential for large increases in CH_4 emissions are a particular concern since CH_4 strongly impacts both atmospheric chemistry and climate [13]. Estimates of the impact of permafrost carbon emissions on future global temperatures range from ∼0.1–0.2°C [14] to 0.3 ± 0.2°C [11] by 2100, with increased carbon emissions expected to continue after 2100 [11].

Recent global inversion studies find no evidence for increasing CH_4 emissions from these regions in the last 10 years [15, 16], despite warming, as indicated by earlier studies [17, 18, 19] and some biogeochemical models [14]. Surface flux observations in the pan-Arctic during 1996–2000 have ranged widely and measurement locations have changed, making it difficult to detect any trend over those years [20], cf. [21].

The present paper derives estimates of CH_4 surface fluxes in Alaska from May to September 2012, based on an extensive program of regional-scale airborne measurements of atmospheric CH_4, the Carbon in Arctic Reservoirs Vulnerability Experiment (CARVE). We quantify the monthly mean CH_4 emissions from Alaska during the growing season, providing a snapshot of the interactions between climate and the vast reservoir of preserved organic matter in the Arctic.

Methods

Measurements. Measurements were made on board a NASA C-23B aircraft (N430NA) during the last two weeks of each month between May and September 2012. Flights were based in Fairbanks, Alaska, USA and ranged from 60.21–71.56°N and 164.5–143.6°W, covering three major regions: 1) the North Slope, which included transits to Barrow and Deadhorse on the northern coast; 2) the Lower Yukon region following the course of the Yukon river south and west of Fairbanks, including the Yukon Delta National Wildlife Refuge (which includes the Yukon and Kuskokwim deltas) and the Innoko National

Reserved for Publication Footnotes

Wildlife Refuge; and 3) the Upper Yukon region which included the Yukon Flats National Wildlife Refuge (grey points in Fig. 1). Each flight lasted 4–10 hours, with the majority of sampling occurring below 200 m above ground level (agl). One or more vertical profiles reaching a maximum of 5500 m above sea level (asl) were flown during each flight, with the maximum height determined by weather conditions. In total, 200 flight hours were flown over 31 flight days.

Two independent cavity ringdown spectrometers measured *in situ* greenhouse gas mole fractions every ∼2.5 s with two separate on board calibration standards for each unit. The first spectrometer measured CO_2, CH_4 and H_2O (Picarro, G1301-m) directly from the inlet. This sensor sampled one of the two calibration gas cylinders every 30 min and is similar to the instrument described by Karion et al.[22]. For the second instrument, ambient air first passed through a Nafion dryer followed by a dry ice trap which effectively lowered the dewpoint to approximately 195 K, before being sampled by the spectrometer. This sensor reported CO_2, CH_4 and carbon monoxide (CO) mixing ratios (Picarro, G2401-m) and sampled both its calibration cylinders every 30 min. The time series used in our analysis merge the CH_4 data from these two instruments, enabling us to fill in gaps when an instrument was calibrating or malfunctioning. Further discussion on the comparison of these two instruments can be found in the SI. Other relevant measurements made on board include ozone (O_3) mixing ratios (2B Technologies, model 205), dewpoint temperature (Edgetech, Vigilant), outside air temperature (Harco, 100366-18), pressure (Paroscientific, 745-15A) and location using a global positioning unit (Crossbow, NAV420).

Model description. Aircraft measurements were aggregated horizontally every 5 km and vertically in 50 m intervals below 1 km asl and 100 m intervals for measurements above 1 km, giving ∼23,000 data points. Each of these points at (x,y,z,t) was treated as a receptor for the Stochastic Time-Inverted Lagrangian Transport (STILT) model [23], which traces the trajectory of the air parcel at each receptor location backward in time over the preceding 10 days and quantifies in space and time where upstream surface fluxes influenced the measured concentrations. Particles are advected by the large-scale (i.e. explicitly resolved) wind field, as simulated by the Advanced Research version of the Weather Research and Forecasting (WRF) model (v3.4.1)[24] on a 3.3 km grid in the innermost domain over Alaska, plus stochastic motions to simulate turbulence. To improve prediction of the meteorological fields in the Arctic, basic options from the Polar variant of WRF [25, 26, 27] were implemented. A two-dimensional influence field ("footprint") is available for each particle every 3 h over its 10 day travel period, representing the response of the receptor to a unit emission of tracer at each grid square (converted unit of ppb / (mg m^{-2} d^{-1})). The footprints used in this analysis were on a 0.5° × 0.5° grid. Further details of both the WRF and STILT models can be found in Henderson et al. [28]. Figure S1 shows the sum of all footprints for the vertical profiles (see below) used in the analysis.

CH_4 fluxes derived from column analysis. Our primary analysis focuses on applying the WRF-STILT framework to the partial column integrals of CH_4 mole fractions measured during vertical profiles, subtracting the background value for air flowing in from outside the study region (the State of Alaska). This "column enhancement" represents the mass loading of the atmosphere from the ground to the top of the residual layer (the maximum height influenced by surface emissions during transit from the boundary) due to emissions in the region. The advantage of this approach is that results are only dependent on the large scale simulation of the vertical structure of the atmosphere, reducing our reliance on the detailed structure of the boundary and residual layers, fine scale variations of emissions at the surface, and turbulent transport elements in the lower atmosphere.

Atmospheric column enhancements have been used in previous studies of CO_2 in the Amazon [29, 30], based on the concept that this quantity measures the total amount of trace gas added to the atmosphere during the transit of an air mass over the land. Similar to Chou et al. [29], we used the CH_4 mole fraction measured at the top of the residual layer height as our background value. The top of the residual layer is effectively equivalent to the bottom of the free troposphere and was identified by comparing the vertical profiles of CH_4, CO_2, CO, O_3 and water vapor (P_{H_2O}). For each vertical profile, the height at which the slope changes sign for each chemical compound was compared and used to determine the residual layer height for that profile. The height at which Alaskan land ceased to influence the column was also assessed using WRF-STILT and contributed to the identification of the residual layer height when there were discrepancies between different chemical compounds. The dashed purple line in Fig. 2 shows the top of the residual layer for a sample profile. Vertical profiles over Alaska from the NOAA measurements on board the Alaska Coast Guard flights [22] during this same period were consistent with the inferred background concentrations.

Column enhancements below the residual layer height ($E_{CH_4,obs}$) were calculated by block averaging the observed CH_4 mole fraction ($[CH_4]$) from each vertical profile into 250 m altitude bins, subtracting the concentration at the top of the residual layer ($[CH_4](h)$) and then integrating the density-weighted concentration enhancements:

$$E_{CH_4,obs} = \int_0^h ([CH_4]\,(z) - [CH_4](h)) \times \frac{P_{air}(z) - P_{H_2O}(z)}{RT(z)} dz,$$

where P_{air}, T and R are the ambient pressure, temperature and universal gas constant, respectively. The column enhancement is illustrated by the black hatch in Fig. 2A. A similar calculation is used to determine the column enhancement from WRF-STILT assuming a unit flux from land $E_{CH_4,unit}$. The mean surface flux associated with each profile ($\overline{F_{\mathrm{CH_4,VP_i}}}$) is then calculated as $\overline{F_{\mathrm{CH_4,VP_i}}} = E_{CH_4,obs}/E_{CH_4,unit}$. The overall mean was calculated by averaging the $\overline{F_{\mathrm{CH_4,VP_i}}}$ for all vertical profiles weighted by their corresponding footprints. Monthly means were calculated in a similar manner but using only profiles from that month. A comparison of surface influences between profiles can be seen in Fig. S2. The red hatch in Fig. 2A shows the modeled column enhancement calculated from the mean monthly surface flux determined from the bootstrapping analysis described below. The mean emission for a given region ($\overline{F_{\mathrm{CH_4,A}}}$, where A is the region of interest) is determined by weighing $\overline{F_{\mathrm{CH_4,VP_i}}}$ for every vertical profile by the portion of the corresponding footprint influence in that region ($I_{A,\mathrm{VP_i}}$), such that

$$\overline{F_{\mathrm{CH_4,A}}} = \frac{\sum_i \overline{F_{\mathrm{CH_4,VP_i}}} \times I_{A,\mathrm{VP_i}}}{\sum_i I_{A,\mathrm{VP_i}}}.$$

To determine the uncertainties in the derived fluxes, observed parameters used in the calculation (measured mole fraction, pressure, temperature, water vapor) were bootstrapped by randomly sampling 1000 times with replacement at each 250 m altitude bin. The residual layer height, which also determines the background concentration, was also sampled 1000 times assuming a uniform probability of the true residual layer height being ± 500 m of the determined height. A second

method of determining the uncertainty compared the calculated mean flux with $\overline{F_{CH_4,VP_i}}$ for each vertical profile. Figure S2 in the SI shows this comparison with the mean monthly fluxes. Results are similar for the overall mean. The average uncertainty from this method lies within the uncertainty determined from our bootstrapping analysis.

Of the 50 vertical profiles from the 2012 campaign, 30 were well-suited for deriving CH_4 flux from the land surface in Alaska (locations shown in black points in Fig. 1 and times given in Table S1). Profiles were rejected due to a) influences by biomass burning (increase in CO of at least 40 ppb within the residual layer) (four profiles); b) significant land influences (>30%) from outside the CARVE study region, usually from Siberia (10 profiles); or c) undefined residual layer, either because the maximum height of the aircraft was too low or the atmospheric structure was too complex for this simple analysis (six profiles).

Land elevation categories derived from ecoregions. The United States Geological Survey and Environmental Protection Agency identifies 20 Level III ecoregions in Alaska [31]. For the purposes of our CH_4 surface-atmosphere flux calculations, these 20 ecoregions were grouped into four categories based on elevation: Highlands (plateaus and uplands); Lowlands (plains, lowlands and flats); the North Slope (Arctic coastal plain and Arctic foothills); and Mountains (ranges and mountains) (colored regions in Fig. 1, complete list in SI). This grouping was used because CH_4 fluxes depend on water table depth and elevation [32, 33] and the atmospheric data in this study cannot resolve all 20 ecoregions. The ecoregions were gridded to $0.5^\circ \times 0.5^\circ$ to match the resolution of the STILT footprints.

Results and Discussion

Results of the column analysis. The black circle in Fig. 3A shows the overall mean CH_4 flux estimates from Alaska if we adopt a uniform emission rate for all land surfaces during each month: 8 ± 2 mg CH_4 m^{-2} d^{-1}, where the uncertainty is the 95% confidence interval from the bootstrapping analysis described above. This baseline assessment does not reflect actual emissions at the surface, but it is determined independent of any assumed surface map and is the most robust number derived from our calculations. Flux estimates were also determined if the Mountains category was assumed to not contribute to CH_4 emissions, which increases the flux from other land types by ∼25% to 10±2 mg CH_4 m^{-2} d^{-1} (red triangle in Fig. 3A). Uncertainties in Fig. 3 show the 95% confidence interval derived from the bootstrapping analysis. These flux estimates represent all land emission processes: biogenic, anthropogenic, and geologic/thermogenic (including possible thermogenic seeps arising from thawing permafrost [3]), but exclude emissions from biomass fires and any ocean processes. These fluxes correspond to an overall emission of 2.1 ± 0.5 Tg CH_4 from May–September, 2012.

Mean fluxes for the entire study period were derived for the three broad land categories (Highlands, North Slope and Lowlands) as shown in Fig. 3A. The CH_4 flux from the Lowlands are consistently greater than from the Highlands, and both of these regions emit significantly more CH_4 than the North Slope ($p < 0.001$ in a paired t-test). This result is consistent with the Lowlands being wetter than the Highlands and the North Slope being cooler, with a thinner active soil layer, than the other regions.

The seasonality of CH_4 fluxes derived over the entire state is shown in Fig. 3B and exhibits an increase in emissions from May to July followed by a gradual decrease until September. The overall range is only 5 mg CH_4 m^{-2} d^{-1}, which is weaker than the 14–80 mg CH_4 m^{-2} d^{-1} difference that can be observed over a season at ground sites [7, 34]. The CH_4 column enhancements sampled by the CARVE aircraft are influenced by emissions from land types heterogeneous in elevation, soil moisture, and organic substrate, as well as diverse seasonal characteristics. (Even at altitudes below 200 m agl, footprints can span a distance of > 500 km.) The large sampling area for each profile tends to dampen seasonal signals that may be observed at individual ground sites with more coherent seasonality.

The seasonal variation observed in our study is generally consistent with other regions in North America [7, 34] and with northern wetland emissions diagnosed from global inversion studies [15, 16, 17]. We observe neither the pattern observed at Zackenberg, Greenland, with high spikes in CH_4 fluxes during the spring thaw and fall freeze up [35], nor as predicted for the Yukon River Valley [36]. Sampling began before the spring thaw, so widespread bursts at that time should have been seen, but it is possible that we did not sample late enough in the season to capture CH_4 bursts in the fall, or that these bursts are more localized in time and space than can be detected by our flight program.

CH_4 fluxes estimated from CH_4:O_3 covariance. We developed a second independent method to estimate CH_4 fluxes using the observed covariance of CH_4 and O_3 in the lowest 1500 m of the atmosphere. These flux estimates are independent of the WRF-STILT footprints, and use the collected data merged at 5 s, resulting in ∼40,000 data points rather than just the vertical profiles. This method heavily weights the particular flight tracks, and involves many simplifying assumptions; it is included to check the order of magnitude of the estimates calculated from the vertical profile analysis. Altitudes closest to the surface can be treated as a constant flux layer, where concentration changes of a chemical compound are dominated by surface exchange with little influence from atmospheric flux divergence. Near the surface in the Arctic, O_3 loss is dominated by dry deposition and *in situ* chemistry can be neglected [37, 38]. Similar to the column analysis, influences from biomass burning were removed by excluding data when absolute CO mole fractions exceeded 150 ppb [39]. At the scale of our measurements, we can assume that O_3 is effectively lost through dry deposition from the same surfaces that emit CH_4, and we can use similarity theory to independently determine CH_4 flux: $F_{CH_4} = F_{O_3} \times (\Delta CH_4/\Delta O_3)$, where F_x is the flux of compound x. Ozone flux is computed from the deposition velocity (v_D) as $F_{O_3} = -v_D \times [O_3]_{500}$, where $[O_3]_{500}$ is the average O_3 mole fraction in the lowest 500 m agl. Figure 4 shows O_3 and CH_4 mole fraction deviations from 10 minute means in the lowest 1500 m agl for June (see Fig. S3 for other months). The slope of the line ($\Delta O_3/\Delta CH_4$) is determined using standard major axis regression [40] and is used to calculate F_{CH_4}, shown in the red circles of Fig. 5. We used a constant O_3 $v_D = -0.3 \pm 0.1$ cm s^{-1}, as determined by Henderson et al. [28] which is consistent with measurements reported over fens, Scots pine forests and tundra [41, 42, 43]. Using this v_D with WRF-STILT footprints results in the modeled O_3 shown in the red triangles in Fig. 2B, reasonably consistent with observations.

The domain-wide average F_{CH_4} from this method is estimated to be 15±5 mg CH_4 m^{-2} d^{-1} for May–September 2012, where the uncertainty reflects the range of O_3 v_D in the literature and the calculated v_D (-0.3 ± 0.1 cm s^{-1}) [28]. Ozone v_D is expected to vary seasonally [43] since it is dependent on the reactivity of O_3 with leaves. Applying the seasonally-varying v_D determined by Henderson et al. [28] (0.13, 0.28,

0.44, 0.35, 0.34 cm s^{-1} for May–September 2012, respectively, with ∼33% uncertainty) results in the estimated F_{CH_4} shown in the black triangles of Fig. 5 (mean=16±5 mg CH_4 m^{-2} d^{-1}). The resulting seasonal cycle is not dissimilar to that calculated using the column analysis in Fig. 3 although the peak of the emissions is later. Overall, the CH_4 flux estimated from its covariance with O_3 is remarkably close to the mean value determined from all of Alaska if mountains were excluded (10 ± 2 mg CH_4 m^{-2} d^{-1}), which is most comparable since we seldom flew near the surface in mountainous terrain. The general agreement between these two independent estimates of CH_4 fluxes increases our confidence in the overall analysis.

Comparison with other flux observations. Our regional flux estimates integrate over wet and dry areas uniformly, giving a more objective regional flux than upscaling from chambers or towers which are typically deployed in areas expected to be significant CH_4 sources. To compare our estimates with these other studies that are sensitive to smaller spatial scales, a distribution map [44] was used to infer the emission rate for wetlands, effectively restricting the areal extent from which CH_4 was emitted and assuming that other CH_4 sources are negligibly small. Resulting emissions are seven times higher than the overall regional mean (56^{+22}_{-13} mg CH_4 m^{-2} d^{-1}) and follow a similar seasonal pattern. This value is similar to CH_4 fluxes measured via airborne eddy covariance during the Arctic Boundary Layer Experiment which took place over the Yukon-Kuskokwim River Delta in southwest Alaska 28 July to 9 August, 1988 (51^{+34}_{-26} mg CH_4 m^{-2} d^{-1} [45]).

Flux measurements determined from static chambers in Alaska range from 0–300 mg CH_4 m^{-2} d^{-1} (compiled by Olefeldt et al. [46]), with a median over 90 studies of 49 mg CH_4 m^{-2} d^{-1}, and eddy-covariance and gradient tower measurements in tundra regions range from 3–80 mg CH_4 m^{-2} d^{-1}, with a median over 13 studies of 34 mg CH_4 m^{-2} d^{-1} (see Table S1). A recent aircraft study over northern Sweden determined CH_4 fluxes equivalent to 29 ± 12 mg CH_4 m^{-2} d^{-1} for a flight in July 2012 over extensive wetland areas [47]. Our values are consistent with these previous measurements once the sampling differences are taken into account.

Comparison with models and inversion studies. Our integrated CH_4 emission estimate of 2.1 ± 0.5 Tg CH_4 over May–September, 2012 falls within the 0.7–6 Tg CH_4 range of emissions estimated from an ensemble of ten different global bottom-up models for the same region and months (Table 1). Our findings are also consistent with the 1.5±0.2 Tg CH_4 estimated by Carbon Tracker-CH_4 [16] and the 1.3±0.3 Tg CH_4 estimated by TM5-4DVAR when biomass burning is excluded [15] for May–September. Our mean is very close to the mean of all the comparable values in Table 1 (2.1 vs. 2.3 Tg CH_4). Uncertainties in Table 1 are 2σ of the emissions from the averaging period. The global inversion study by Chen and Prinn [17] estimates an annual emission of 2±1 Tg CH_4 from Alaska if 17% of North American wetlands are assumed to be in Alaska, as stated in their source map [48]. Our value can be used as a lower-bound for total emissions in 2012, and if we assume that 50% of annual CH_4 emissions occurs between October and April, as reported for a site in Greenland [35], then the upper-bound for emissions in 2012 would be 4 ± 1 Tg CH_4. A reasonable annual estimate for 2012 is the mean of these two bounds, 3 ± 1 Tg CH_4, and is consistent with assuming that emissions for the months of October and November are similar to August and September and that emissions in the remaining months are near zero.

Our results are lower than emissions reported in a recent study of the Yukon River Valley [36], which gave an annual emission of 4.01 Tg CH_4 yr^{-1} for this region alone, which comprises 30% of Alaska. Likewise, the annual emissions from Alaskan thermogenic seeps have been reported to be 1.5–2 Tg CH_4 yr^{-1} [3]. This value would comprise at least 50–67% of the total annual Alaskan emissions. Both of these estimates seem to be higher than can be accommodated by our observations.

Summary and Conclusions

CARVE is the first study to make frequent and sustained airborne measurements of CH_4 over large areas of Arctic and boreal Alaska throughout the growing season. We derived emissions of 2.1 ± 0.5 Tg CH_4 from Alaska during May to September 2012, and we found that the Lowland and Highland regions consistently emitted CH_4 at higher rates than the North Slope. A modest seasonal cycle was observed over all regions, with fluxes roughly doubling from May to July, then decreasing gradually in August and September. Stronger seasonality was likely not observed because the atmosphere integrates over heterogeneous land-types with asynchronous seasonal cycles. Analysis of CARVE 2013 measurements is under way, with 2014 measurements currently taking place. Comparing the results from these additional years with their different environmental forcing may allow the factors affecting emissions at a regional-scale to be determined.

The total estimated CH_4 emitted from the region (2.1 ± 0.5 Tg CH_4 over May–September 2012) is quite small compared to the global emissions of 550 Tg CH_4 yr^{-1} [21] (<0.5%), despite the recent warming of permafrost areas in Alaska. Since this is the first top-down regional study of Alaska based on observations, we cannot directly assess whether emissions have increased in response to climatic shifts. However, our results are consistent with fluxes obtained in recent global top-down inversion studies, which reported a lack of recent trends in CH_4 emission in the Arctic [15, 16, 18, 19]. Our work and these studies together indicate that CH_4 emissions from Arctic tundra regions have not contributed significantly to increasing levels of global CH_4 observed during the last decade. Our work during the growing season of 2012 in Alaska provide the baseline against which possible future increases in Arctic boreal and tundra CH_4 emissions can be assessed.

ACKNOWLEDGMENTS. The research described in this manuscript was performed as part of the Carbon in Arctic Reservoirs Vulnerability Experiment (CARVE), an Earth Ventures (EV-1) investigation, under contract with the National Aeronautics and Space Administration (NASA). We acknowledge funding from NOAA and NSERC Canada (PDF Fellowship to RC). Computing resources for this work were provided by the NASA High-End Computing (HEC) Program through the NASA Advanced Supercomputing (NAS) Division at Ames Research Center. We thank the CARVE Science team for helpful discussion, and P. Bergamaschi, X. Zhu, Q. Zhuang, C. Koven and J. Melton and the WETCHIMP team for sharing their model output. We also thank the pilots, flight crews and NASA Airborne Science staff from the Wallops Flight Facility for enabling the CARVE science flights.

1. Schuur EAG, et al. (2008) Vulnerability of Carbon to Climate Change: Implications for the Global Carbon Cycle. BioScience 58:701–714.
2. Shakhova N, et al. (2010) Extensive methane venting to the atmosphere from sediments of the East Siberian Arctic Shelf. Science 327:1246–50.
3. Walter Anthony KM, Anthony P, Grosse G, Chanton J (2012) Geologic methane seeps along boundaries of Arctic permafrost thaw and melting glaciers. Nat. Geosci. 5:419–426.
4. Tarnocai C, et al. (2009) Soil organic carbon pools in the northern circumpolar permafrost region. Global Biogeochem. Cy. 23:1–11.
5. Hansen J, Ruedy R, Sato M, Lo K (2010) Global surface temperature change. Rev. Geophys. 48:2010RG000345.
6. Romanovsky VE, Smith SL, Christiansen HH (2010) Permafrost thermal state in the polar Northern Hemisphere during the international polar year 2007-2009: a synthesis. Permafrost Periglac. 21:106–116.
7. Worthy DEJ, Levin I, Hopper F, Ernst MK, Trivett NBA (2000) Evidence for a link between climate and northern wetland methane emissions. J. Geophys. Res. 105:4031–4038.
8. Schuur EAG, et al. (2009) The effect of permafrost thaw on old carbon release and net carbon exchange from tundra. Nature 459:556–9.
9. Harden JW, et al. (2012) Field information links permafrost carbon to physical vulnerabilities of thawing. Geophys. Res. Lett. 39:L15704.
10. Hodgkins SB, et al. (2014) Changes in peat chemistry associated with permafrost thaw increase greenhouse gas production. P. Natl. Acad. Sci. USA.
11. Schaefer K, Lantuit H, Romanovsky VE, Schuur EAG, Witt R (2014) The impact of the permafrost carbon feedback on global climate. Environ. Res. Lett. 9:085003.
12. Schuur EAG, et al. (2013) Expert assessment of vulnerability of permafrost carbon to climate change. Climatic Change 119:359–374.
13. Holmes CD, Prather MJ, Sovde OA, Myhre G (2013) Future methane, hydroxyl, and their uncertainties: key climate and emission parameters for future predictions. Atmos. Chem. Phys. 13:285–302.
14. Gao X, et al. (2013) Permafrost degradation and methane: low risk of biogeochemical climate-warming feedback. Environ. Res. Lett. 8:035014.
15. Bergamaschi P, et al. (2013) Atmospheric CH4 in the first decade of the 21st century: Inverse modeling analysis using SCIAMACHY satellite retrievals and NOAA surface measurements. J. Geophys. Res. 118:7350–7369.
16. Bruhwiler L, et al. (2014) CarbonTracker-CH_4: an assimilation system for estimating emissions of atmospheric methane. Atmos. Chem. Phys. 14:8269–8293.
17. Chen YH, Prinn RG (2006) Estimation of atmospheric methane emissions between 1996 and 2001 using a three-dimensional global chemical transport model. J. Geophys. Res. 111:D10307.
18. Rigby M, et al. (2008) Renewed growth of atmospheric methane. Geophys. Res. Lett. 35.
19. Dlugokencky EJ, et al. (2009) Observational constraints on recent increases in the atmospheric CH4 burden. Geophys. Res. Lett. 36:L18803.
20. McGuire AD, et al. (2012) An assessment of the carbon balance of Arctic tundra: comparisons among observations, process models, and atmospheric inversions. Biogeosciences 9:3185–3204.
21. Kirschke S, et al. (2013) Three decades of global methane sources and sinks. Nat. Geosci. 6:813–823.
22. Karion A, et al. (2013) Long-term greenhouse gas measurements from aircraft. Atmos. Meas. Tech. 6:511–526.
23. Lin JC, et al. (2003) A near-field tool for simulating the upstream influence of atmospheric observations: The Stochastic Time-Inverted Lagrangian Transport (STILT) model. J. Geophys. Res. 108:doi:10.1029/2002JD003161.
24. Skamarock WC, et al. (2008) A Description of the Advanced Research WRF Version 3., (National Center for Atmospheric Research, Boulder, CO), Technical Report June.
25. Hines KM, Bromwich DH (2008) Development and Testing of Polar Weather Research and Forecasting (WRF) Model. Part I: Greenland Ice Sheet Meteorology*. Mon. Weather Rev. 136:1971–1989.
26. Bromwich DH, Hines KM, Bai L (2009) Development and testing of Polar Weather Research and Forecasting model: 2. Arctic Ocean. J. Geophys. Res. 114:D08122.
27. Hines KM, Bromwich DH, Bai LS, Barlage M, Slater AG (2011) Development and Testing of Polar WRF. Part III: Arctic Land. J. Climate 24:26–48.
28. Henderson J, et al. (submitted) Atmospheric transport simulations in support of the Carbon in Arctic Reservoirs Vulnerability Experiment (CARVE). Atmos. Chem. Phys. Discuss.
29. Chou WW, et al. (2002) Net fluxes of CO_2 in Amazonia derived from aircraft observations. J. Geophys. Rese. 107:4614.
30. Gatti LV, et al. (2014) Drought sensitivity of Amazonian carbon balance revealed by atmospheric measurements. Nature 506:76–80.
31. Gallant A, Binnian E, Omernik J, Shasby M (1995) Ecoregions of Alaska, U.S. Geological Survey Professional Paper 1567., Technical report.
32. Zhuang Q, et al. (2007) Net emissions of CH4 and CO2 in Alaska: Implications for the region's greenhouse gas budget. Ecol. Appl. 17:203–212.
33. Zona D, et al. (2009) Methane fluxes during the initiation of a large-scale water table manipulation experiment in the Alaskan Arctic tundra. Global Biogeochem. Cycles 23.
34. Harazono Y, et al. (2006) Temporal and spatial differences of methane flux at arctic tundra in Alaska. Memoirs of National Institute of Polar Research, Special Issue 59:79–95.
35. Mastepanov M, et al. (2008) Large tundra methane burst during onset of freezing. Nature 456:628–30.
36. Lu X, Zhuang Q (2012) Modeling methane emissions from the Alaskan Yukon River basin, 19862005, by coupling a large-scale hydrological model and a process-based methane model. J. Geophys. Res. 117:1–11.
37. Jacob DJ, et al. (1992) Summertime Photochemistry of the Troposphere at High Northem Latitudes. J. Geophys. Res. 97:16421–16431.
38. Walker TW, et al. (2012) Impacts of midlatitude precursor emissions and local photochemistry on ozone abundances in the Arctic. J. Geophys. Res. 117:D01305.
39. Liang Q, et al. (2011) Reactive nitrogen, ozone and ozone production in the Arctic troposphere and the impact of stratosphere-troposphere exchange. Atmos. Chem. Phys. 11:13181–13199.
40. Jolicoeur P (1990) Bivariate allometry: interval estimation of the slopes of the ordinary and standardized normal major axes and structural relationship. J. Theor. Biol. 144:275–285.
41. Jacob DJ, et al. (1992) Deposition of Ozone to Tundra. J. Geophys. Res. 97:16473–16479.
42. Tuovinen J-P, Aurela M, Laurila T (1998) Resistances to ozone deposition to a flark fen in the northern aapa mire zone. J. Geophys. Res. 103:16953–16966.
43. Mikkelsen T, et al. (2004) Five-year measurements of ozone fluxes to a Danish Norway spruce canopy. Atmos. Environ. 38:2361–2371.
44. Bergamaschi P, et al. (2007) Satellite chartography of atmospheric methane from SCIAMACHY on board ENVISAT: 2. Evaluation based on inverse model simulations. J. Geophys. Res. 112:D02304.
45. Ritter JA, et al. (1992) Airborne Flux Measurements of Trace Species in an Arctic Boundary Layer. J. Geophys. Res. 97:16601–16625.
46. Olefeldt D, Turetsky MR, Crill PM, McGuire AD (2013) Environmental and physical controls on northern terrestrial methane emissions across permafrost zones. Glob. Change Biol. 19:589–603.
47. O'Shea SJ, et al. (2014) Methane and carbon dioxide fluxes and their regional scalability for the european arctic wetlands during the mamm project in summer 2012. Atmos. Chem. Phys. Discuss. 14:8455–8494.
48. Fung I, et al. (1991) Three-dimensional model synthesis of the global methane cycle. J. Geophys. Res. 96:13033–13065.
49. Melton JR, et al. (2013) Present state of global wetland extent and wetland methane modelling: conclusions from a model inter-comparison project (WETCHIMP). Biogeosciences 10:753–788.
50. Riley W, et al. (2011) Barriers to predicting changes in global terrestrial methane fluxes: analyses using CLM4Me, a methane biogeochemistry model integrated in CESM. Biogeosciences 8:1925–1953.
51. Zhu X, Zhuang Q, Qin Z, Glagolev M, Song L (2013) Estimating wetland methane emissions from the northern high latitudes from 1990 to 2009 using artificial neural networks. Global Biogeochem. Cycles 27:592–604.
52. Matthews E, Fung I (1987) Methane emissions from natural wetlands: Global distribution, area, and environmental charactersitics of sources. Global Biogeochem. Cycles 1:61–86.

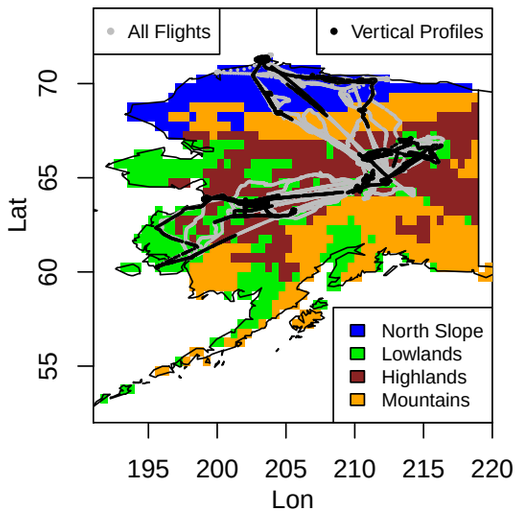

Fig. 1. Location of flight tracks (grey) and vertical profiles (black) during CARVE 2012. Background colours are elevation categories based on US EPA Level III ecoregions.

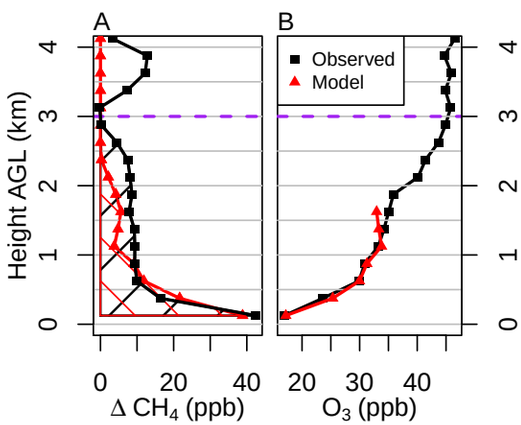

Fig. 2. Sample CH_4 vertical profile used for column analysis and corresponding O_3 profile from 22 September 2012. Dashed purple line is the identified top of the residual layer and hatched areas are used to determine the column enhancement.

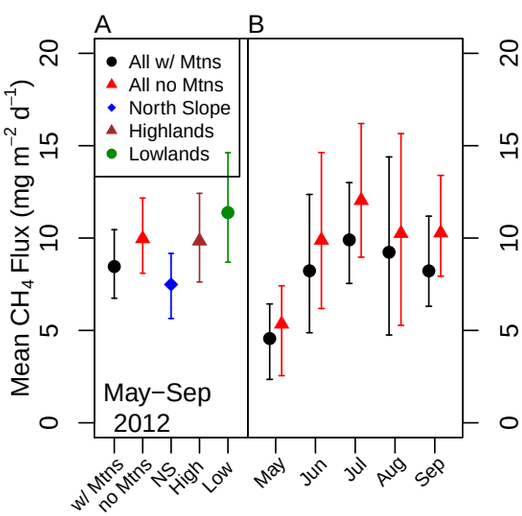

Fig. 3. Estimated mean CH_4 fluxes from the column analysis for (A) the entire study period (May–September 2012) and (B) by month.

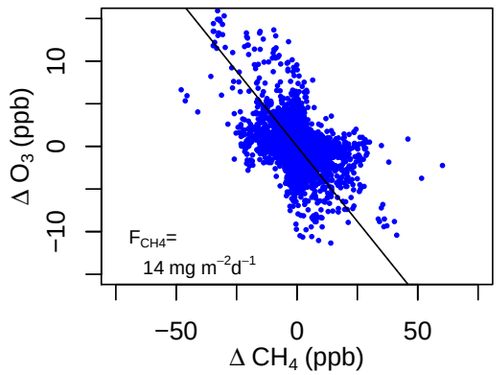

Fig. 4. Covariance of O_3 and CH_4 below 1500 m agl for June. See SI for other months.

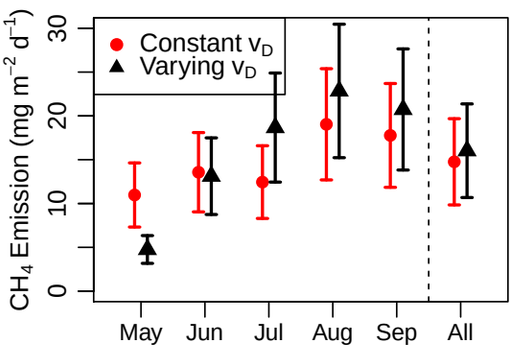

Fig. 5. Estimated methane fluxes from the O_3:CH_4 analysis assuming a constant and seasonally-varying O_3 v_D, red and black points, respectively. Error bars reflect the uncertainty in the O_3 v_D ($\sim$33%).

Table 1. Methane emissions from various models for the region 55–75°N, 141–169°W for May–Sep of the given years, except TEM which was run for all of Alaska and the given value is the annual emission

Lead author	Model	Emissions (Tg)	Averaging Period	Ref
Land surface models				
Melton	DLEM	0.8±0.2	1993–2004	[49]
Melton	LPJ-Bern	1.2±0.3	1993–2004	[49]
Melton	LPJ-WHyMe	6±1	1993–2004	[49]
Melton	LPJ-WSL	0.9±0.2	1993–2004	[49]
Melton	ORCHIDEE	1.0±0.4	1993–2004	[49]
Melton	SDGVM	0.7±0.2	1993–2004	[49]
Riley	CLM4Me	5±2	2001–2010	[50]
Zhu		2.6±0.1	2000–2009	[51]
Zhuang	TEM	3 (annual)	1980–1996	[32]
Matthews		4.34		[52]
Inverse models				
Bergamaschi	TM5-4DVAR	1.3±0.3	2001–2010	[15]
Bruhwiler	CT-methane	1.5±0.2	2000–2009	[16]
Chen	MATCH	2±1	1996-2001	[17]
This study		2.1±0.5	2012	

Supplemental Information for "Methane emissions from Alaska in 2012 from CARVE airborne observations"

Rachel Y.-W. Chang, Charles E. Miller, Steven J. Dinardo, Anna Karion, Colm Sweeney, Bruce C. Daube, John M. Henderson, Marikate E. Mountain, Janusz Eluszkiewicz, John B. Miller, Lori M. Bruhwiler, Steven C. Wofsy

September 29, 2014

S1 Comparison of the two spectrometers

The water vapor correction for the G1301 model was calibrated in the laboratory before deployment. The water vapor levels throughout the study ranged from 0.013–1.8%, resulting in a correction for CH_4 and CO_2 of 0.013-1.9% and 0.016–2.3%, respectively, with average corrections of 16 ppb for CH_4 and 3.8 ppm for CO_2. No water vapor correction was applied to measurements from the G2401 model because the sample is dried in that system and water vapor levels were less than 0.001%. For the entire 2012 study, the difference between the two instruments was on average 0.7±2.7 ppb for CH_4 and 0.3±0.4 ppm for CO_2, where the uncertainty is the standard deviation. This gives us confidence in the water vapor correction, since the differences between the instruments are not correlated with water vapor and the water vapor correction is much greater. This result is consistent with previous studies in the literature detailing the water vapor correction for Picarro cavity ring down systems [1, 2]. The merged time series used in this study was based on the measurements from the G2401 and missing measurement points (e.g. due to calibration) were filled in by the G1301 offset by the mean difference between the two instruments for each flight.

S2 Elevation categories based on ecoregions

The 20 Level III ecoregions defined by the United States Environmental Protection Agency [3] were grouped into four elevation categories: North Slope (Arctic Coastal Plain, Arctic Foothills); Highlands (Interior Forested Lowlands and Uplands, Interior Highlands and Klondike Plateau, Copper Plateau); Lowlands (Subarctic Coastal Plain, Seward Peninsula, Bristol Bay Nushagak Lowlands,

Aleutian Islands, Interior Bottomlands, Yukon Flats, Cook Inlet, Coastal Western Hemlock Sitka Spruce Forests); and Mountains (Brooks Range / Richardson Mountains, Ogilvie Mountains, Alaska Range, Wrangell and St. Elias Mountains, Ahklun and Kilbuck Mountains, Alaska Peninsula Mountains, Pacific Coastal Mountains).

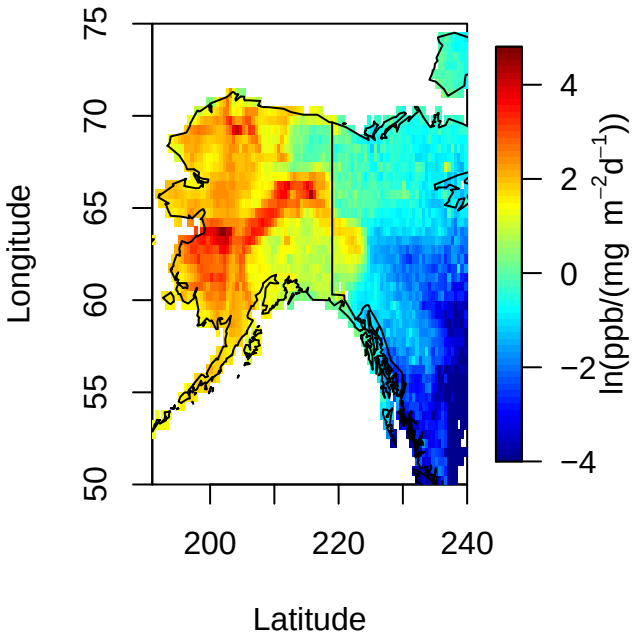

Figure S1: Surface influence of 30 vertical profiles used in this analysis.

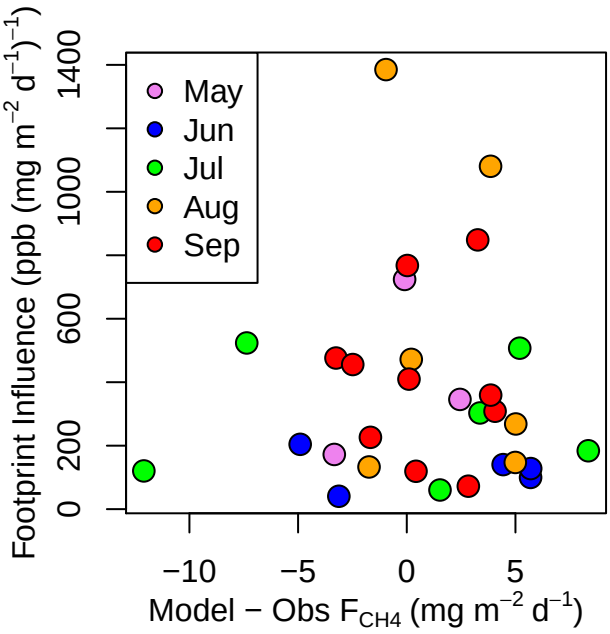

Figure S2: Difference between mean monthly flux and $\overline{F_{\mathrm{CH_4,VP_i}}}$ and corresponding footprint influence used in the weighted-average.

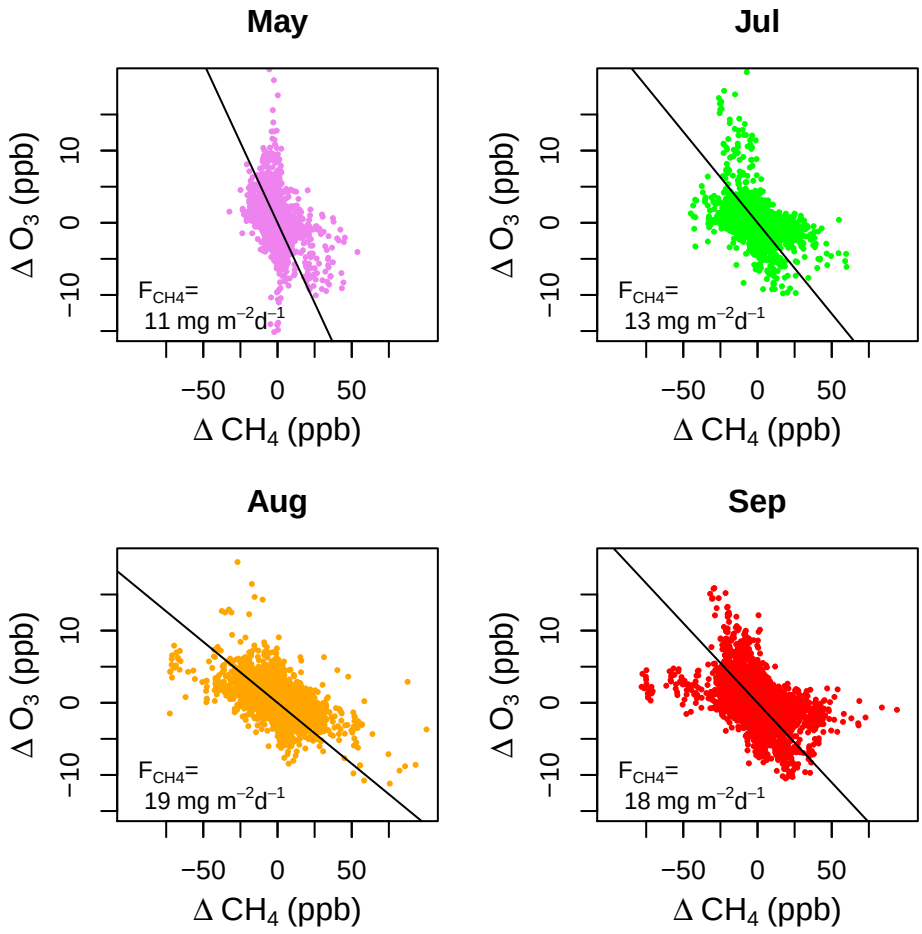

Figure S3: Covariance of O_3 and CH_4 below 1500 m agl for each month and corresponding CH_4 flux.

Table S1: Details of vertical profiles used in analysis (dates in days since Jan 1)

Date	Start Date (UTC)	End Date (UTC)	Residual Layer Height (m)
20120523	143.838	143.878	4000
20120527	147.932	147.970	2300
20120601	152.866	152.950	3000
20120621	172.875	172.981	1900
20120622	173.765	173.824	1600
20120622	173.973	173.987	3000
20120624	175.882	175.895	5000
20120624	175.896	175.910	2500
20120717	198.775	198.871	3000
20120717	199.004	199.057	3200
20120722	203.881	203.905	1800
20120722	203.905	204.051	1800
20120725	206.857	206.895	1300
20120725	206.925	207.058	1200
20120814	226.762	226.784	2100
20120814	226.785	226.855	3200
20120819	231.984	232.028	3100
20120821	233.772	233.876	2400
20120822	234.771	234.960	1800
20120823	236.106	236.150	2900
20120919	262.855	262.868	4000
20120919	262.869	262.898	2100
20120921	264.913	265.027	3800
20120922	265.865	265.914	3000
20120922	265.919	265.991	3000
20120924	267.859	268.086	2000
20120924	268.086	268.170	2600
20120926	270.034	270.045	2500
20121001	275.013	275.025	2250
20121001	275.100	275.199	2300

Table S2: Methane emissions from tower measurements in tundra regions

Location	Lat	Lon	Land Type	Year	Flux (mg/m2/d)	Reference
Yukon Delta	61.09	-162	Tundra and Lake	1988	25	[4]
Happy Valley	69.17	-148.85	Wet Tundra	1995	80.2	[5]
Kuparuk Bay	69.51	-148.23	Wet Tundra	1996	3.3	[5]
Zackenberg	74.5	-21	Fen	1997	86.5	[6]
Barrow	71.32	-156.62	Wet Tundra	1999	68.7	[5]
Barrow	71.32	-156.62	Wet Tundra	2000	29.9	[5]
Barrow	71.32	-156.62	Wet Tundra	2001	34.3	[5]
Siberia	72.37	-126.5	Wet Tundra	2006	18.7	[7]
Barrow	71.28	-156.6	Wet Tundra	2007	24.6	[8]
Greenland	74.47	-20.57	Fen	2008	78.7	[9]
Greenland	74.47	-20.57	Fen	2009	52	[9]
Barrow	71.28	-156.6	Wet Tundra	2009	32	[10]
Barrow	71.28	-156.6	Wet Tundra	2011	37.3	[11]

References

[1] Chen H, et al. (2010) High-accuracy continuous airborne measurements of greenhouse gases (CO_2 and CH_4) using the cavity ring-down spectroscopy (CRDS) technique. *Atmos. Meas. Tech.* 3:375–386.

[2] Rella CW, et al. (2013) High accuracy measurements of dry mole fractions of carbon dioxide and methane in humid air. *Atmos. Meas. Tech.* 6:837–860.

[3] Gallant A, Binnian E, Omernik J, Shasby M (1995) Ecoregions of Alaska, U.S. Geological Survey Professional Paper 1567., Technical report.

[4] Fan SM, et al. (1992) Micrometerological Measurements of CH_4 and CO_2 Exchange Between the Atmosphere and Subarctic Tundra. *J. Geophys. Res.* 97:16627–16643.

[5] Harazono Y, et al. (2006) Temporal and spatial differences of methane flux at arctic tundra in Alaska. *Memoirs of National Institute of Polar Research, Special Issue* 59:79–95.

[6] Friborg T, Christensen TR, Hansen BU, Nordstroem C, Soegaard H (2000) Trace gas exchange in a high-arctic valley 2 . Landscape CH 4 fluxes measured and modeled using eddy correlation have measurements. *Global Biogeochem. Cycles* 14:715–723.

[7] Sachs T, Wille C, Boike J, Kutzbach L (2008) Environmental controls on ecosystem-scale ch4 emission from polygonal tundra in the lena river delta, siberia. *J. Geophys. Res.* 113.

[8] Zona D, et al. (2009) Methane fluxes during the initiation of a large-scale water table manipulation experiment in the Alaskan Arctic tundra. *Global Biogeochem. Cycles* 23.

[9] Tagesson T, et al. (2012) Land-atmosphere exchange of methane from soil thawing to soil freezing in a high-Arctic wet tundra ecosystem. *Glob. Chang. Biol.* 18:1928–1940.

[10] Sturtevant CS, Oechel WC, Zona D, Kim Y, Emerson CE (2012) Soil moisture control over autumn season methane flux, Arctic Coastal Plain of Alaska. *Biogeosciences* 9:1423–1440.

[11] Sturtevant CS, Oechel WC (2013) Spatial variation in landscape-level CO2 and CH4 fluxes from arctic coastal tundra: influence from vegetation, wetness, and the thaw lake cycle. *Glob. Chang. Biol.* 19:2853–66.